Proceedings of the Canadian Society for Mechanical Engineering International Congress 2021
CSME Congress 2021
June 27-30, 2021, Charlottetown, PE, Canada

ON THE LARGE EDDY SIMULATION OF TWIN ROUND JETS WITH CLOSE PROXIMITY: THE EFFECTS OF REYNOLDS INEQUALITY

M. Karami[1*], S. Ramezani[2], H. Tofighian[3]
[1]Reticom Solutions Inc., Windsor ON, Canada
[2]Department of Mechanical Engineering, Concordia University, Montreal QC, Canada
[3]Department of Mechanical Engineering, Amirkabir University of Technology, Tehran, Iran
*mkarami@reticom.ca

Abstract— The LES study of twin round jets for very close vicinity (S/D=1.1) are presented using OpenFOAM, an open source CFD package. The effect of the jets' Reynolds number inequality is studied by setting one jet's Re to 10,000 and changing the other's from 10,000 to 5,000. The validation of numerical results is assessed by comparing the single jet simulation with the available experimental data that shows a reasonable agreement in terms of radial and axial distributions of RMS and mean velocity. Two different concentrations for the jets are used as virtual ink to study the behavior of turbulent mixing in the jet core and shear layers. Results show that the air flow from quiescent medium heading toward the jet cores enters the jet from the inner shear layer and develop four counter-rotating vortices, which evolve as moving downstream up to break up the jets. Lowering one jet's Re is found to reduce the breakup length for both jets, including the one with fixed Re. As one jet's Re decreases, the stronger jet tends to penetrate into the weaker one by means of high radial velocity component. The root-mean-squares of axial velocity components show three local maximum at the shear layer, where the latter demonstrates a similar pattern to that of concentration.

Keywords-Lage Eddy Simulations, Round Jet, Twin Jets, Numerical Simulation, Jet Interference

I. INTRODUCTION

Parallel jets have a wide range of industrial applications including burners, cooling and heating system, air conditioners and pollutant disposal devices. Twin parallel jets are one of the most extensively used group of parallel jets and have been broadly employed for cooling as well as fuel injection systems. Twin Parallel jets can be classified into various categories based on the jet ejection geometry such as twin planar jets and twin round jets. The key observation in most of the applications is the entrainment of ambient fluid into the core of the jets and as a result, increased mixing which is due to the higher momentum transfer. Reviewing the literature proves that there have not been as many numerical researches on twin round jets compared to the twin planar jets in spite of the fact there have been several experimental studies in this area to explain the coupling relationship of the jets. Extensive studies reveal that the jet mixing performance can be affected dramatically by initial conditions like nozzles type [1, 2], Reynolds number [3] and turbulence intensity [4]. Okamoto et al. [5] studied the self-similar transformation process of turbulent twin round jet with spacing distance S/D=5 and 8.06, experimentally and clarified that the twin round jet contains an elliptic form while interacting with each other through the self-similar formation process. Harima et al. [6] performed a series of experiments on turbulent twin round jets with a spacing distance of S/D=2, 4 and 8 to investigate the turbulence intensity field. They revealed that due to the interference between two circular jets the development of the streamwise turbulence intensity at each jet center is suppressed and this effect is less observed on the mean streamwise velocity. Yimer [7] studied the strong-jet/weak-jet coupling experimentally and numerically by utilizing flow visualization to explain the interaction of unequal jets and behavior of vortical structures accurately. The mean and root-mean-squared (r.m.s) velocities of CFD results across the jet closely followed the experiment, while the weak jet's trajectory is poorly predicted. Faghani [8] developed a semi-analytical model, called "Bending Model" to predict the interaction, trajectory, and attachment of twin round jets. The results were in reasonable agreement with the k-ε numerical simulations as well as experimental results available in literature. To date, despite several experimental investigations in this area, to the best of the authors' knowledge, there have been fewer high fidelity numerical simulations like LES (Large Eddy Simulations) on the unequal twin round jets in a very closed proximity which have remarkable applications in burner industry [9,10]. Thus, the objective of this paper is to study the interference of the twin-round jets with together located at very close vicinity and to investigate the impact of unequal injection on the evolution of coherent structures as well as interaction of two jets by flow visualization techniques like injection of passive scalars. For this purpose, two-round jets at close neighborhood are investigated numerically by LES containing a left jet as a strong jet with the Reynolds number (Re) of 10,000 and varying the right jet's Re from 5,000 to 10,000. Due to the lack of experimental study for selected configurations with the same flow characteristics, the LES results of an additional case with a single jet are examined with the experimental data [11].

II. NUMERICAL PROCEDURES

Filtered incompressible Navier-Stokes equations as well as continuity equation govern the turbulent flow of twin round jets in the present LES study. The dimensionless forms of the filtered equations are expressed in (1) and (2) [12].

$$\frac{\partial \widetilde{u_i}}{\partial x_i} = 0 . \tag{1}$$

$$\frac{\partial \widetilde{u_i}}{\partial t} + \frac{\partial \left(\widetilde{u_i}\widetilde{u_j} \right)}{\partial x_j} = -\frac{\partial \tilde{p}}{\partial x_i} + \frac{1}{\mathrm{Re}} \frac{\partial^2 \widetilde{u_i}}{\partial x_j^2} - \frac{\partial^2 ij}{\partial x_j} . \tag{2}$$

Here, $\tilde{u}_i$, $\tilde{p}$ and *Re* represent the dimensionless filtered of the i^{th} velocity component, filtered pressure and Reynolds number, respectively. The effect of the small scales on the larger scales is hidden in the sub-grid scale (SGS) shear stress tensor in (2), τ_{ij}. The characteristic length and velocity in the definition of the *Re* number and dimensionless variables are the jet's diameter (D) and left (strong) jet's exit velocity, correspondingly. Boussinesq approach and Dynamic one-equation LES model [13] are engaged to determine the SGS shear stress (τ_{ij}). To track the interference of the twin jets on each other in the current work, different passive scalars with uniform profiles, namely c_L and c_R are ejected from the left and right nozzles, respectively. Thus, two filtered concentration equations which are expressed in dimensionless format (see (3)) should be involved in the equations of interest.

$$\frac{\partial \tilde{c}}{\partial t} + \frac{\partial \left(\widetilde{u_i}\tilde{c} \right)}{\partial x_j} = \frac{1}{Sc\,\mathrm{Re}} + \frac{\neg_{sgs}}{\neg Sc_{sgs}\,\mathrm{Re}} . \tag{3}$$

Where, v_{sgs}, Sc and Sc_{sgs} are the SGS eddy viscosity, Schmidt number and SGS Schmidt number with the values of 0.7 and 0.4 for the latter two parameters in the present simulation, respectively. The open-source software package, OpenFOAM, is issued to discretize the incompressible Navier-Stokes equations by Finite Volume Method (FVM) within the incompressible solver pimpleFoam. Both the convection and diffusive terms are discretized by 2nd-order central scheme, while a Second Order Upwind Euler (SOUE) scheme is employed for the transient terms. The computational domain is composed of a main cylinder, with 20D length and 20D diameter, and two pipes with the distance of *S/D=1.1* which are attached to the main cylinder as shown in Fig. 1. The pipes have fully-developed turbulent profile at their inlet, with 6.5D length (based on the authors' knowledge) to let the inlet white noise shape the physical vortices. Due to the narrow gap between the jets, a novel approach is utilized to generate a high-quality block structure hexahedral mesh for this computational domain resulting nearly 3,000,000 cells for all investigated cases, which has been carried out after grid-independence study. The y^+ adjacent to all walls are kept below 1 based on the suggestion of the reference books [14]. A summary of the applied boundary conditions is displayed in Table I.

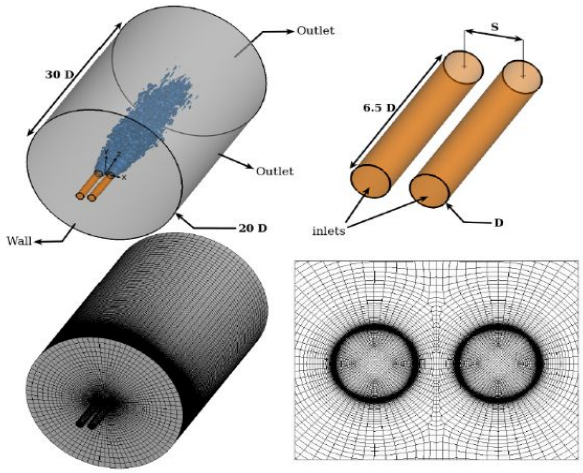

Figure 1. Computational domain of the present LES simulation of twin round jets and corresponding grid topology

TABLE I. SUMMARY OF BOUNDARY CONDITIONS [14]

	Velocity	***Pressure***	***Passive sclaer concentration***
Inlet of Jets	White noise with 10% turbulence intensity and fully-developed profile	Zero-gradient	Unifrom profile
Wall	No-slip	Zero-gradient	Zero-gradient
Outlet	Zero-gradient	Fixed-value	Neumann condition for the outlet fluid and Dirichlet condition for the inlet

At the outlet, the pressure is assumed to be equal to the ambient pressure while the zero-gradient condition is used for velocity since the domain is large enough. To investigate the effect of the jets' power inequality, three various cases are considered (see Table II). The right-to-left jet velocity ratios (u_R/u_L) are set to 0.5, 0.75 and 1 for Case1, Case2 and Case3, respectively. The jet spacing is set to S/D=1.1 for all the cases. Due to the lack of the experimental data to validate the LES results for twin-jets with the spacing of *S/D=1.1*, Case0 with a single jet injection comprising the same mesh quality, is utilized for which the jet is injected from left side with the *Re=5000*. The LES results of the single jet are compared with the experimental study of He et al. [11] which are presented in Fig. 2 and Fig. 3. Fig. 2 exhibits the mean and RMS values of the axial velocity (z-velocity component) against the measured data of He et al. [11] at two different axial locations z/D=2, 6. As it is observable, the mean velocity profiles matches with the benchmark data remarkably, while the turbulence intensity comparison at z/D=2 (closer section to the jet exit) demonstrates non-negligible misalignments. This mismatch is thought to be the artifact of eddy generations by white noise (WN) at the pipe inlet, which leads to the collapse of eddies inside the pipe before reaching the jet exit section. This discrepancy between the present LES and the experiment [11] for the turbulence intensity is gradually eliminated by moving further downstream (z/D=6). Next, the comparison of the mean axial velicty (z-velocity) profile along the jet axis (x=y=0) with the measured data of He et al. [11] is shown in Fig. 3. The trend is captured correctly whereas some underpredictions are detectable after z/D=5 by moving downstream.

TABLE II. REYNOLDS NUMBER OF SIMULATED TEST CASES

Case Name	Case0	Case1	Case2	Case3
Left Jet Reynolds Number	5,000	10,000	10,000	10,000
Right Jet Reynolds Number	0	5,000	7,500	10,000

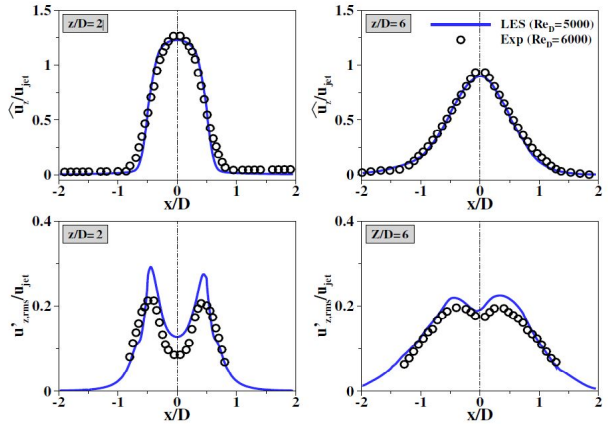

Figure 2. Evaluation of mean z-velocity (axial, Top row) as well as RMS axial velocity (bottom row) against the experimental data of He et al. [11] at two different downstream locations z/D=2 and 6.

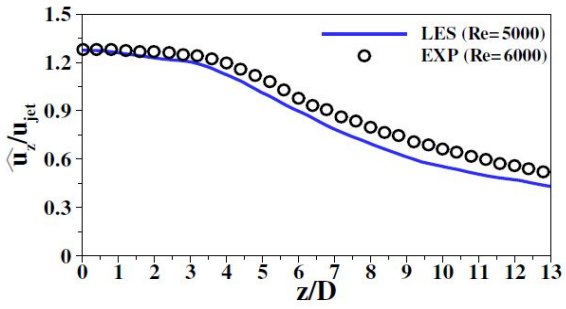

Figure 3. Comparison of mean axial (z-direcion) velocity with the experimental data of He et al. [1s1] along the jet axis (x=y=0)

III. RESULTS AND DISCUSSION

Fig. 4 demonstrates the distribution of Q-criterion (which is helpful to identify the vortical structures in turbulent flows [14]) colored by the concentration for Case1. As mentioned earlier two different passive scalars (i.e., c_L and c_R) are injected from the jet exits to study the scalars convection of two jets, simultaneously. Here, the concentrations of left and right jets are illustrated by blue and red colors, respectively. The green color indicates the concentration of quiescent medium which is zero for either c_L or c_R. Owing to implementing white noise (WN) as the source of turbulence generator at the jet inlet pipe, the coherent structures are not observed at the jet exit. As advancing toward downstream, the flow instabilities causing by jets' shear layer tend to increase that consequently rises the turbulence level of the flow field. Hence, increasing level of the interference of the vortical structures of both jets can be seen in Q-criterion getting away from jets' exit.

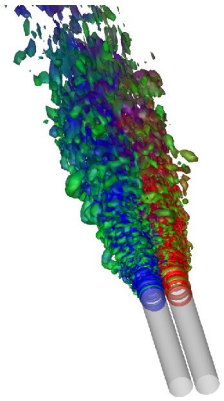

Figure 4. Instantaneous iso-surfaces of Q-criterion coloured by concentration (blue: c_L, red: c_R, Ggreen: quiesent medium) for Case1

Fig. 5 displays the contours of mean and instantaneous normalized axial velocity for Cases 1 to 3. The mean-velocity vectors at various cross-sections (i.e., different z/D values) are also superimposed on the velocity contours. Due to the same Re numbers of both jets for Case3, a symmetric pattern for mean velocity contours as well as vectors is observable. Additionally, the instantaneous velocity contour depicts a similar evolution of vortical structures of both jets for this case. Due to the presence of high momentum flow at the jet exits in Case3, the jets show less tendency to transfer momentum with the quiescent medium and try to keep their cylindrical shape. While, getting far from the jet exits, the flow instabilities become stronger which leads to growth of turbulence level that consequently yields to rise in momentum transfer via larger vortical structures. Study of mean flow vectors at different cross sections indicates the flow behavior which has not been pointed out yet. Meslem et al. [15] showed the distribution of the axial velocity of the twin jets at different cross sections which demonstrates a similar trend detectable in the velocity vectors of Fig. 4, of course they neglected the radial velocity component (i.e., x-velocity). The vectors show the gradual mixing of the jets as the z/D increases for Case3. In the region between two jets (inner shear layer), an interesting phenomenon can be seen when the radial velocity of the jets is diverging at z/D=1 while they tend to converge to each other after jets' breakup (z/D=4). The comparison of mean flow vectors of Case1 (with highest inequality of Re), Case2 and Case3 (equal twin-jets) proves that: the weaker right jet, the more tendency of the left jet to be deviated toward right one. For instance, at section z/D=2 the velocity vectors of three cases exhibit the highest and least amount of deflection of the vectors of left jet toward right one for Case1 and Case3, respectively. Another important finding is the effect of the right jet Re on the breakup location of the stronger jet. While the left jet has the same Reynolds number from Case3 to Case1, it seems that reducing the right jet Reynolds number will result in quicker jet breakup in the left jet. The left jet breakup occurs at z/D of ~4, ~3.5, ~3 for Case3, Case2, and Case1, correspondingly. This can be explained by considering both jets as a one unique jet as they are located very close together. This is true especially for Case3 where both jets have the same Re of 10,000.

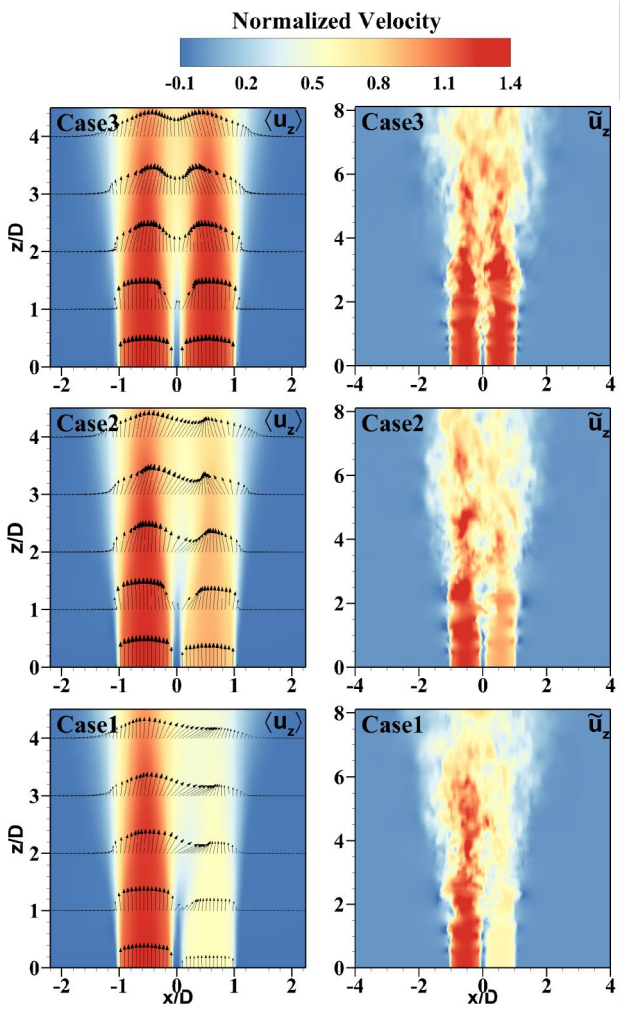

Figure 5. Comparison of mean (Left) and instantaneous (Right) streamwse velocity contours for Case3 (Top), Case2 (Middle) and Case1 (Bottom)

The mean velocity vectors of Case1 show a different pattern comparing to the other studied cases. Since the breakups of both jets occurs faster, the diverging behavior of velocity vectors of jets at the inner shear layer (as distinguishably seen for Case3) cannot be observed here. Moreover, the radial velocity component direction is from the left jet to the right one, which is becoming intensified as moving toward downstream and mainly affect the velocity distribution of the left half of the weaker jet.

Fig. 6 depicts the streamlines superimposed on the distribution of the mean axial vorticity at different cross sections perpendicular to the streamwise direction (i.e., z/D =constant) for Case1 and Case3. This plot is useful to describe what we observed in Fig. 5 before. For z/D=1.5 of Case3, one can see all streamlines are upcoming from the quiescent ambient toward the jet centers due to low-pressure region caused by jet shear layer. It is useful to mention a fundamental difference between the twin planar jets and twin round jets that the former has a very strong low-pressure region between two jets, while the latter does not experience a similar low-pressure region since the flow has the chance to enter from the quiescent medium into the inner shear layer from all directions. The flow entering the inner shear layer plays an important role in mixing of the jets. At z/D=1.5, a very poor mixing can be observed since the momentum of the jets is still strong. One can see two contour-rotating vortices in each jet, caused by the entering flow from quiescent medium. At the centerline, (i.e., y/D=0) the streamlines of both jets are oriented toward outside region, which results in observing diverging velocity vectors that are seen in corresponding section of Fig. 5, at z/D=1. Moving downstream, the turbulent structures cause more jet mixing, which can be identified via bigger vortices inside the jet region. At z/D=4, the jets have completely been broken up and the streamlines freely pass the inner shear layer border and transfer momentum and mass from one jet to another. It can also be seen that at the centerline, the streamlines of the jets are oriented toward the inner region, which is compatible to the observation of converging velocity vectors in Fig. 5. For Case1 at z/D=1.5, no counter-rotating vortices are observed in the left jet (stronger) while they exist in the right jet. The flow direction is mostly from the left jet to the right one, as seen in Fig. 5. Moving toward downstream, the x-velocity becomes stronger from left jet to the right one so that at z/D=4 the flow field is dominated by radial streamlines originated from the left jet center to all over the near field while in the far field there is still flow from quiescent medium toward the center point. Fig. 7 demonstrates the distribution of mean axial velocity at the mid plane for different z/D values for cases 1 to 3. As seen in fig. 5, results of case 3 are symmetric for both jets while a different pattern can be seen for those of case 1. Furthermore, moving toward downstream one can observe how the jets are gradually mixed by each other and the quiescent medium. It can also be seen that the peak velocity of the left jet at z/D=9 is higher for case 3 comparing to that of case 1, which means that the left jet seems to have more momentum in case 3, which can be explained by the effect of one jet momentum to the other that was mentioned before.

Fig. 7 demonstrates the distribution of mean axial velocity at the mid plane for different z/D values for cases 1 to 3. As seen in Fig. 5, results of case 3 are symmetric for both jets while a different pattern can be seen for those of case 1. Furthermore, moving toward downstream one can observe how the jets are gradually mixed by each other and the quiescent medium. It can also be seen that the peak velocity of the left jet at z/D=9 is higher for case 3 comparing to that of case 1, which means that the left jet seems to have more momentum in case 3, which can be explained by the effect of one jet momentum to the other that was mentioned before.

Fig. 8 depicts the normalized distribution of RMS of axial and radial (x-velocity) velocity fluctuations at different locations for all simulated cases. For z/D=3 with developing shear layer, all curves show three local maximums which are associated with three shear layers; two outer shear layers at the interface of two jets with the quiescent medium and one inner shear layer (the inner shear layers of two jets are mixed together) in the region between the jets (inner zone). The peak value in the outer shear layers is proportional to the jets' Re number.

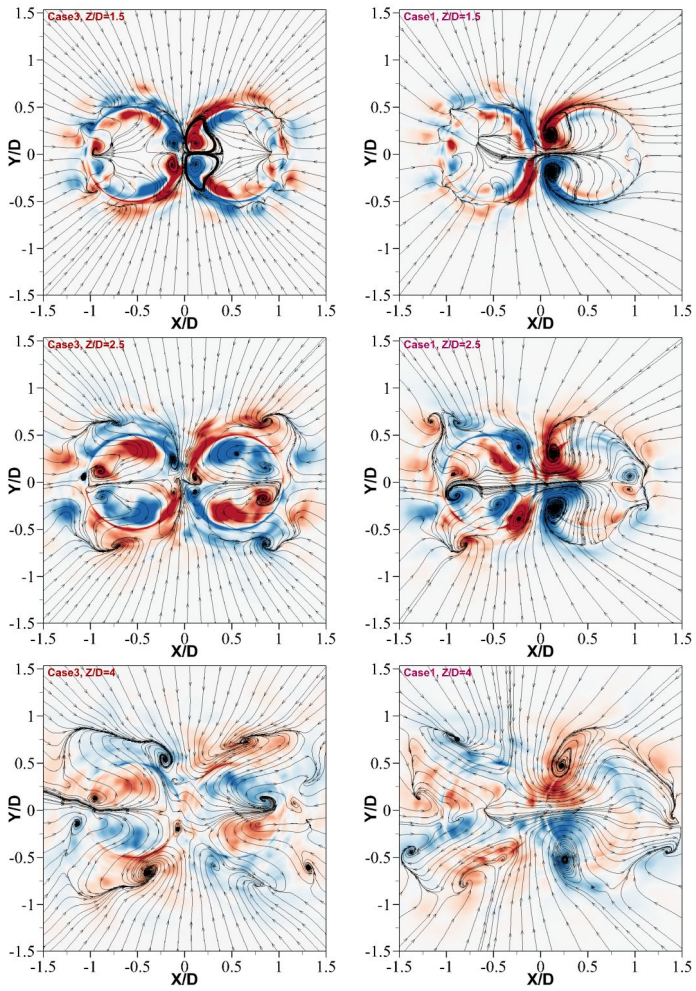

Figure 6. Contour of mean axial vorticity along with the streamlines at different perpendicular cross sections for case 1 and case 3.

In fact, regarding the left jet, despite a very close vicinity of the two jets, the strong jet (left) for all cases is not affected by the right one for all sections; hence the fluctuations profiles demonstrate very reasonable similarity for the outer shear layer of the left jet for three cases.

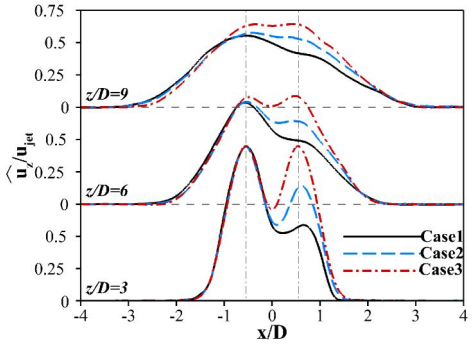

Figure 7. Comparison of the mean streamwise velocity in three downstream locations (z/D=3,6 and 9) for three cases; Case1 (solid lines), Case2 (dashed lines) and Case3 (dash-dotted lines)

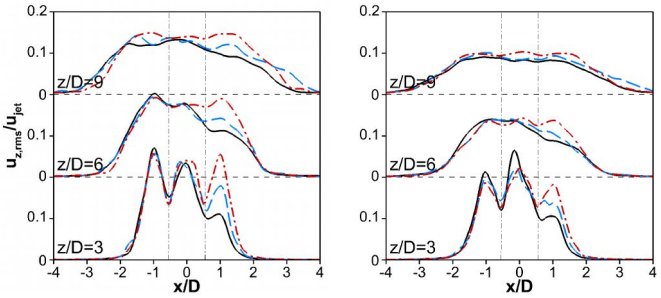

Figure 8. Comparison of the RMS values of z-velocity fluctuations for three cases; Case1 (Top), Case2 (Middle) and Case3 (Bottom) in three downstream locations: solid lines (z/D=3), dashed lines (z/D=6) and dash-dotted (z/D=9)

A huge difference is detectable between the outer shear layer fluctuations peaks of the right jet for three cases. Another interesting point is that turbulence intensity of x-velocity fluctuations at the inner zone (-0.5<x/D<0.5) is way more than outer shear layers for each case which is in contrast with the fluctuations of axial velocity in the inner region. Moving toward downstream, the RMS values of three cases tend to become similar which demonstrates the rise in mixing of the two jets; also, fluctuations tend to decrease as a result of jet dissipation and corresponding weaker shear layers.

Fig. 9 displays the mean concentration profiles of left and right jets at three different axial locations, z/D=3, 6 and 9 for all three cases. The profiles of mean concentration of left jet ($\widehat{c_L}$) demonstrate that moving from highest inequality of twin-jets exit (Case1) to equal ones (Case3) does not affect significantly the main trajectory of the stronger jet (left) for all cases. However, the inner shear layer ($0<x-x_L<1.5$) concentration of stronger jet (left) is diminished as the right jet becomes stronger (from Case1 to Case3). An evidence of this behavior is that the variations of the left and right jets' concentrations versus inequality are in opposite direction. In fact, in the inner shear layer zone of the right jet, moving from weak right jet to stronger one (Case1 to Case3) right passive scalar tends to occupy less quota. Another interesting point is that getting far away from the jet exit relocates the maximum point of the concentration of both left and right jets for all cases in diverging direction. In addition, the left jet's maximum point for three cases coincides approximately at all axial sections. However, regarding the right jet the maximum point of the mean concentration (Fig. 9, right) experiences a dramatic displacement from Case3 to Case1 (shifts outward direction) and moving toward downstream intensifies this displacement. This can be justified by the velocity vectors of Fig. 4 which prove that for Case1 the deflection of the velocity vectors from left jet to right one pushes the weaker jet outward direction.

Fig. 10 exhibits the RMS of concentration fluctuations of two jets at two axial locations (z/D=3 and 6) for two cases, Case1 and Case3. $(c_L)_{rms}$ and $(c_R)_{rms}$ represent the left and right concentration fluctuations, respectively. The first note is that: except the $(c_R)_{rms}$ for Case1 at z/D=3, the fluctuations at the inner zone is higher than the outer shear layers; this is because the x-velocity fluctuations which are mainly responsible for the mixing of the passive scalars are greater in inner zone compared to the outer zones' values (see Fig. 8, $u_{x,rms}/u_j$ profiles).

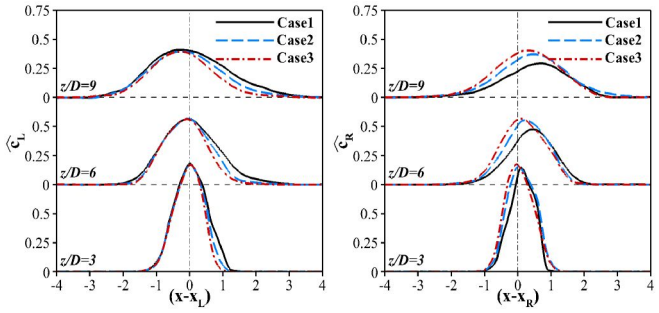

Figure 9. Comparison of the mean concentration fields of passive scalars in three downstream sections (z/D=3, 6 and 9) for three cases; Case1 (solid lines), Case2 (dashed lines) and Case3 (dash-dotted lines). Left: passive scalar injected from left jet, Right: passive scalar injected from right jet.

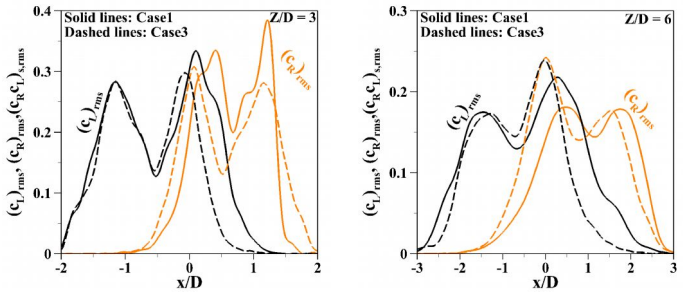

Figure 10. Comparison of the root mean square of concentration field's fluctuations in two downstream locations, z/D=3 and 6, for two cases; Case1 (solid lines), Case3 (Dashed lines)

It is worth mentioning that the velocity fluctuations in x direction are compatible with the concentartion gradient direction which results in intensified concentration fluctuations at the inner zone relative to the outer one. The comparable profiles of $(c_L)_{rms}$ for two cases in all sections proves that the strong jet (left)'s outer shear layer is less influenced by the right jet; however, in the inner zone close to the jet exit (z/D=3), $(c_L)_{rms}$ and $(c_R)_{rms}$ of Case1 is larger than Case3 which mimic the x-velocity fluctuations' behavior at this section. Further downstream (z/D=6) the $(c_L)_{rms}$ and $(c_R)_{rms}$ for Case1 will be slightly smaller than the Case3 that is compatible with the $u_{x,rms}/u_j$ profiles of Fig. 8 as well.

IV. Conclusion

The flow dynamics of very closed positioned twin round jets (S/D=1.1) was studied by enganing LES approach. The effects of jets momentum inequality on the mass and momentum transfer were also investigated by setting on jet Re to 10,000 and changing the Re of the other jet from 10,000 to 5,000. Lowering the Re of the one jet was found to not only reduce the jet breakup of that jet, but it also make the other jet to experience breakup in shorter diatance, that can be explained by the fact that the very close jets behave similar to one unique jet and lowering the one jet's Re will result in lower momentum and quicker breakup, consequently. The streamline of the perpendicular plane show a very complicated pattern of the flow, where the flow is oriented from the quiescent medium toward jet centers, and the jet mixing strats from the inner shear layer located between two jets. At short streamwise distance from jets exit plane, the air flow from the quiescent medium penetrates both jets' high momentum core and develop two counter-rotating vortices in each of them, which result in appearance of diverging radial velocity components. As moving forward, the evolutionary of these vortices causes a convergent radial velocity in the centerplane of two jets, and they eventually result in jet breakup. For high value of Re inequality of the jets (Case1), a strong radial flow can be seen from high Re jets to the weaker one, which make it tilted toward the oouter reagion. The RMS values of velocity and concentration fields show three local maximums, two outer shear layes and one inner layer. As moving downstream, the transportation of momentum results in weaker shear layers and lower RMS values, consequently. The RMS distribution of concentration also demonstrates a similarity to that of radial velocity.

References

[1] J. B. Mi, P. Kalt, G. J. Nathan, and C. Y. Wong, "PIV measurements of a turbulent jet issuing from round sharp-edged plate ," Exp. fluids, Springer, vol. 42(4), pp. 625-637, April 2007.

[2] W. R. Quinn, "Upstream nozzle shaping effects on near field flow in round turbulent free jets," Eur. J. Mech. B Fluids, Elsevier, vol. 25(3), pp. 279-301, May 2006.

[3] I. Namer, and M. V. Ötügen, "Velocity measurements in a plane turbulent air jet at moderate Reynolds numbers," Exp. fluids, Springer, vol. 6(6), pp. 387-399, January 1988.

[4] S. Russ, and P. J. Strykowsk, "Turbulent structure and entrainment in heated jets: the effect of initial conditions," Phys. Fluid Fluid Dynam., AIP Publishing, vol. 5(12), pp. 3216-3225, December 1993.

[5] T. Okamoto, T., M. Yagita, A. Watanabe, and K. Kawamura, "Interaction of twin turbulent circular jet," Bull. JSME, vol. 28(238), pp. 617-622, 1985.

[6] T. Harima, S. Fujita, and H. Osaka, "Turbulent properties of twin circular free jets with various nozzle spacing," Eng. Turb. Modelling Exp. 6, Elsevier Science BV, pp. 501-510, January 2005.

[7] Yimer, I., Becker, H.A. and Grandmaison, E.W., 2001. The strong-jet/weak-jet problem: new experiments and CFD. Combust Flame, Elsevier, vol. 124(3), pp. 481-502, Februray 2001.

[8] E. Faghani, and S. N. Rogak, "A phenomenological model of two circular turbulent jets," INT J. Engine Res., vol. 14(3), pp. 293-304, June 2013.

[9] Y. Han, "Twin-Jet Sprays for Fuel Direct Injection," PhD diss., Friedrich-Alexander-Universität Erlangen-Nürnberg (FAU), 2016.

[10] H. F. Durst, A. Handtmann, M. Weber, and F. Schmid, "Twin-jet nozzle injectors for gasoline engines," MTZ worldwide, Springer, vol. 73(6), pp. 34-40, June 2012.

[11] C. He, Y. Liu, and S. Yavuzkurt, "Large-eddy simulation of circular jet mixing: lip-and inner-ribbed nozzles," Comput Fluids, Elsevier, vol. 168, pp. 245-264, May 2018.

[12] P. Sagaut, Large eddy Simulation for Incompressible Flows: an Introduction, Springer Science & Business Media, Springer Science & Business Media, 2006.

[13] C. Fureby, G. Tabor, H. G. Weller, and A. D. Gosman, "A comparative study of subgrid scale models in homogeneous isotropic turbulence," Phys. Fluids, AIP Publishing , vol. 9(5), pp. 1416-1429, May 1997.

[14] L. Davidson, Fluid mechanics, turbulent flow, and turbulence modeling, 2015.

[15] A. Meslem, A. Dia, C. Beghein, M. El Hassan, I. Nastase, and P. J. Vialle, "A comparison of three turbulence models for the prediction of parallel lobed jets in perforated panel optimization," Build Environ., Elsevier, vol. 46(11), pp. 2203-2219, November 2011.